JOURNAL OF GEOPHYSICAL RESEARCH: SPACE PHYSICS, VOL. 118, 1270–1287, doi:10.1002/jgra.50167, 2013

Ion gyro-harmonic structuring in the stimulated radiation spectrum and optical emissions during electron gyro-harmonic heating

A. Mahmoudian,[1] W. A. Scales,[1] P. A. Bernhardt,[2] A. Samimi,[1] E. Kendall,[3] J. M. Ruohoniemi,[1] B. Isham,[4] O. Vega-Cancel,[4] and M. Bordikar[1]

Received 2 November 2012; revised 3 February 2013; accepted 4 February 2013; published 25 March 2013.

[1] Stimulated electromagnetic emissions (SEEs) are secondary radiation produced during active space experiments in which the ionosphere is actively heated with high power high frequency (HF) ground-based radio transmitters. Recently, there has been significant interest in ion gyro-harmonic structuring the SEE spectrum due to the potential for new diagnostic information available such as electron acceleration and creation of artificial ionization layers. These relatively recently discovered gyro-harmonic spectral features have almost exclusively been studied when the transmitting frequency is near the second electron gyro-harmonic frequency. The first extensive systematic experimental investigations of the possibility of these spectral features for third electron gyro-harmonic heating are provided here. Discrete spectral features shifted from the transmit frequency ordered by harmonics of the ion gyro-frequency were observed for third electron gyro-harmonic heating for the first time at a recent campaign at the High Frequency Active Auroral Research Program (HAARP) facility. These features were also closely correlated with a broader band feature at a larger frequency shift from the transmit frequency known as the downshifted peak (DP). The power threshold of these spectral features was measured, as well as their behavior with heater beam angle, and proximity of the transmit frequency to the third electron gyro-harmonic frequency. Comparisons were also made with similar spectral features observed during second electron gyro-harmonic heating during the same campaign. A theoretical model is provided that interprets these spectral features as resulting from parametric decay instabilities in which the pump field ultimately decays into high frequency upper hybrid/electron Bernstein and low frequency neutralized ion Bernstein IB and/or obliquely propagating ion acoustic waves at the upper hybrid interaction altitude. Coordinated optical and SEE observations were carried out in order to provide a better understanding of electron acceleration and precipitation processes. Optical emissions were observed associated with SEE gyro-harmonic features for pump heating near the second electron gyro-harmonic during the campaign. The observations affirm strong correlation between the gyro-structures and the pump-induced optical emissions.

Citation: Mahmoudian, A., W. A. Scales, P. A. Bernhardt, A. Samimi, E. Kendall, J. M. Ruohoniemi, B. Isham, O. Vega-Cancel, and M. Bordikar (2013), Ion gyro-harmonic structuring in the stimulated radiation spectrum and optical emissions during electron gyro-harmonic heating, *J. Geophys. Res. Space Physics*, *118*, 1270–1287, doi:10.1002/jgra.50167.

1. Introduction

[2] Use of high frequency heating experiments has been extended in recent years as a useful methodology for plasma physicists wishing to remotely study the properties and behavior of the ionosphere as well as nonlinear plasma processes [*Hysell and Nossa*, 2009; *Kosch et al.*, 2007; *Pedersen and Gerken*, 2005; *Pedersen et al.*, 2010]. This technique has also been used extensively to investigate the charged dust layers in the mesosphere [*Chilson et al.*, 2000; *Havnes et al.*, 2003; *Mahmoudian et al.*, 2011; *Mahmoudian and Scales*, 2012]. High power electromagnetic waves transmitted from the ground interact with the local plasma in the ionosphere and can produce stimulated electromagnetic

[1]The Bradley Department of Electrical and Computer Engineering, Virginia Tech, Blackburg, Virginia, USA.

[2]Plasma Physics Division, Naval Research Laboratory, Washington DC, USA.

[3]SRI International, Menlo Park, California, USA.

[4]Department of Natural Sciences and Mathematics, Inter American University of Puerto Rico, Bayamón, Puerto Rico.

Corresponding author: A. Mahmoudian, The Bradley Department of Electrical and Computer Engineering, Virginia Tech, VA 24060, USA. (alirezam@vt.edu)

2169-9380/13/10.1002/jgra.50167

emissions (SEEs) through the parametric decay instability [*Thide et al.*, 1982]. The interaction of the injected radio beam with local plasma may generate different types of waves, instabilities, and turbulence, and as a result a variety of spectral features in the scattered wave are expected. The EM pump wave may undergo a direct conversion in which EM pump decays into a scattered EM and electrostatic (ES) wave. The direct parametric decay instability can be distinguished by strong SEE spectral sidebands. Magnetized stimulated Brillouin scatter (MSBS) which involves decay of the EM pump wave into ion acoustic IA or electrostatic ion cyclotron (EIC) and a scattered EM wave is an example of the direct conversion [*Norin et al.*, 2009; *Bernhardt et al.*, 2009, 2010]. The other possible scenario is the conversion of the EM wave first to a high frequency ES wave and irregularities through the oscillating two stream instability (OTSI) [*Dysthe et al.*, 1983; *Huang and Kuo*, 1995]. The ES wave then decays into another high frequency ES wave and low frequency ES wave. Finally the high frequency ES wave scatters from irregularities back into the EM wave measured on the ground. The downshifted maximum (DM), a distinct peak at a frequency approximately 10 kHz below the pump [*Leyser*, 2001] involving electrostatic lower hybrid waves is believed to be produced through this mechanism [*Bernhardt et al.*, 1994; *Huang and Kuo*, 1995; *Leyser et al.*, 1989, 1990].

[3] The strength and frequency shift of the SEE emission lines are a powerful diagnostic tool to estimate ionospheric parameters and get a sense of the possible physical processes/plasma waves involved in the decay process as well as possible conditions for acceleration of electrons [*Leyser*, 2001]. IA and EIC mode excitation through the MSBS instability can be used to estimate the electron temperature and as ion mass spectrometers to determine the composition of the *E* and *F* layers, respectively [*Bernhardt et al.*, 2009, 2010]. It also has been shown that the spatial scale of striations involved in the formation of the DM and broad upshifted maximum (BUM) can be estimated by measuring the decay rate of the peak intensity of the DM and BUM [*Norin et al.*, 2008].

[4] There has been an extensive recent interest in associated ionospheric processes when the transmitter frequency is tuned to harmonics of the electron gyro-frequency f_{ce} in the ionosphere [e.g., *Pedersen et al.*, 2010, 2011] . Recent studies at the High Frequency Active Auroral Research Program (HAARP) facility, showed new SEE spectral features within 1 kHz of the pump frequency due to so-called Stimulated Ion Bernstein Scatter (SIBS) during pump heating near the second electron gyro-harmonic $2f_{ce}$ [*Bernhardt et al.*, 2011; *Scales et al.*, 2011; *Samimi et al.*, 2012a, 2012b]. SEE spectral structures ordered by harmonics of the ion gyro-frequency f_{ci} (near 50 Hz) were observed. A theory based on the interaction at the reflection altitude was originally proposed by *Bernhardt et al.* [2011] which suggests the parametric decay of O-mode EM pump wave into electron Bernstein (EB) and ion Bernstein (IB) modes. Other observations have shown a new spectral feature associated with SIBS process. A broadband spectral feature, within 1 kHz of pump frequency was observed during heating near $2f_{ce}$ on occasion as well [*Samimi et al.*, 2012a, 2012b]. A new theory based on the interaction at the UH altitude, where the pump frequency equals the local UH frequency, was developed by *Samimi et al.* [2012a, 2012b] which not only was able to explain the ion gyro-structures as a result of SIBS decay process but also predicted the oblique IA decay process as a possible source responsible for broadband spectral features observed in the experiment. The capability of SEE features in predicting irregularities generated during heating experiments can be employed to investigate the generation mechanism and plasma waves involved for other associated processes such as artificial optical emissions.

[5] Artificial airglow is another phenomenon associated with ionospheric heating experiments and creation of visible artificial optical emissions has been reported by *Bernhardt et al.* [1988] and *Pedersen et al.* [2010]. High frequency plasma waves parametrically excited during pump heating near $2f_{ce}$ may cause acceleration of electrons. Superthermal electrons may enhance airglow emissions through the collisional excitation of neutral species [*Bernhardt et al.*, 1988] or even create new plasma when their energy exceeds the ionization potential of gasses [*Gustavsson et al.*, 2006].

[6] Objectives of this investigation include the consideration of the SEE spectral behavior under variable pump power, proximity to the gyro-harmonic frequency nf_{ce}, and beam angle relative to the background magnetic field variation. Also, the relationship between such spectral features and electron acceleration and creation of plasma irregularities is an important focus.

[7] During experimental campaigns at the HAARP facility in 2011 and 2012, excitation of SIBS has been observed for the first time for the pump heating of the ionosphere near the third electron cyclotron frequency $3f_{ce}$. It is observed that the previously observed SEE downshifted peak (DP) feature and the newly discovered ion gyro-structures appear simultaneously in the SEE spectra which may show that these two features are produced with the same physical process but at different altitudes. Further relationship between these features and the well-known DP feature in SEE will be discussed in light of these recent observations.

[8] This paper is organized as follows. In the next section, the experimental procedure is described. Then experimental observations are provided for two experimental campaigns. Next, an analytical model is used to study the parametric decay instability in the interaction region. Parametric decay instability is then considered for a variety of parameters. The impact of (1) the pump field strength, (2) its frequency relative to the electron gyro-harmonic frequency, and (3) angle of the pump field relative to the geomagnetic field on the SEE spectrum are considered. A corresponding mode associated with the broadband feature is investigated. Finally, summary and conclusions are provided.

2. Experimental Procedure

[9] The data from four different experiments performed 21–26 July 2011 and 5–9 August 2012 at the HAARP facility (geographical coordinates 62.39°N, 145.15°W) are presented. The ionospherically scattered EM signal was measured using a 30 m folded dipole antenna and a receiver with around 90 dB dynamic range at a rate of 250 kHz. A large dynamic range HF receiver was set up during the 2011 campaign at HAARP to record stimulated electromagnetic emissions (SEEs). Four measurement sites were used during the 2012 campaign at different locations with respect to the

HF transmitter. The experiments were carried out in O-mode polarization. Different sets of experiments were designed to investigate the effect of the pump field strength, antenna beam angle of transmission, and frequency sweeping near $2f_{ce}$ and $3f_{ce}$.

[10] One set of experiments on 24 July 2011 between 03:58 UT and 04:58 UT was designed to measure the excitation threshold of the SIBS decay instability near $3f_{ce}$. The heater beam was pointed at five different zenith angles to study the variation and the strength of the SIBS emission lines. The zenith angles were 14°, 18°, 21°, 24°, and 27°. The azimuth angle was 200° for all cases. The power was increased from 0.1 MW (which corresponds to effective radiated power (ERP) ≈27 MW) to 3.6 MW (ERP ≈ 1 GW) in 0.1 MW steps every 6 s. The power spectrum of the experiments shows discrete structures both upshifted and downshifted from the pump frequency (4.3 MHz) as soon as the pump power exceeds 0.7 MW (ERP ≈ 190 MW). This was the first observation of SIBS excited near $3f_{ce}$ and will be presented in the next section. Variation of previously observed discrete and broadband features at $2f_{ce}$ with pump frequency sweeping was examined on 25 July 2011 between 5:55 UT and 6:55 UT. The heater beam was pointed at magnetic zenith (zenith angle ZA = 14°, azimuth angle AZ = 200°) and vertical (ZA = 0°, AZ = 200°), and the pump frequency was increased from 2.9 to 2.96 MHz in 20 kHz steps during 45 s "on" and 45 s "off" heating cycles. The HF transmitter was at full power (3.6 MW) corresponding to 300 MW effective radiated power (ERP) at 2.90 MHz. The corresponding spectra show the ion gyro-structures embedded in the broadband feature, broadband feature, discrete structures as well as low frequency ion acoustic IA emission lines associated with the MSBS process.

[11] Experiments during the 2012 campaign were designed to produce SIBS near the $3f_{ce}$. A more detailed study on the effect of the proximity of pump frequency to $3f_{ce}$ and angle of antenna beam was considered. The zenith angle was varied from 14° to 27° in four steps. The azimuth angle was 200° for all cases. The heater duty cycle was 45 s on, 45 s off for the beam pointed at magnetic zenith (MZ) and was 30 s on, 30 s off for all other transmission angles. During all 2012 experiments, the HAARP heater was operated transmitting O-mode continuous wave at full power of 3.6 MW (ERP ≈ 1 GW). In the first set of experiments, the pump frequency was increased from 4.17 to 4.35 MHz in 0.2 MHz steps during 45 s "on" and 45 s "off" heating cycles. This experiment was carried out on 7 August 2012 between 4:30 UT and 5:30 UT.

[12] The last set of experiments was dedicated to a joint observation of optical emissions and SEE to study the physics associated with artificial airglow excited by high power radio waves. Coordinated optical and SEE observations were carried out during the 2012 campaign in order to provide a better understanding of electron acceleration and precipitation processes. Optical emissions were observed with multiple wide- and narrow-field imagers at HAARP during the experiment. Results for correlation between SEE SIBS features and pump-induced optical emissions are provided for pump heating near $2f_{ce}$ during the campaign. The observations affirm strong correlation between the SIBS and the airglow. On 9 August 2012, the HAARP facility was operated at 2.7 MHz between 11:56 and 11:57 UT after sunset, and then the transmitter frequency was increased in 20 kHz steps every 30 s up to 2.9 MHz. The beam was pointed at the MZ (202° azimuth, 14° zenith).

[13] The International Geomagnetic Reference Field (IGRF) model provided the magnetic field strength and direction in the upper atmosphere over HAARP. The magnetic field near the HF reflection altitude is estimated to be $|B| = 5.012Œ10^{-5}$ T for a typical interaction altitude 220 km which was the case during most experiments. This magnetic field corresponds to an ion gyro-frequency f_{ci} near 48 Hz and electron cyclotron frequency of 1.4 MHz.

[14] The ionospheric plasma at *F* region heights above the heater was probed with HF transmissions from the Super-DARN HF radar located at Kodiak, Alaska. This radar detects backscatter when decameter-scale irregularities are present in the ionization.

3. Experimental Results

3.1. Discrete Ion Gyro-Features for $f_0 \approx 3f_{ce}$

[15] Discrete narrowband spectral features within 1 kHz of the pump frequency separated by multiples of the ion gyro-frequency f_{ci} observed in the SEE spectrum have been attributed to the simultaneous parametric decay of upper hybrid/electron Bernstein waves into multiple upper hybrid/electron Bernstein and ion Bernstein waves [*Bernhardt et al.*, 2011, *Scales et al.*, 2011, *Samimi et al.*, 2012a, 2012b]. As stated in section 1, this process will be referred to here as Stimulated Ion Bernstein SIB Scatter (SIBS) [*Bernhardt et al.*, 2011]. Observations of SIBS for the pump frequency f_0 near $3f_{ce}$ are described here for the first time.

[16] The effect of the amplitude of the pump field on SIBS was examined on 24 July 2011 from 4:43 UT to 4:48 UT. The transmitter was operated with 4 min on and 1 min off cycles. The power increased from 0.1 MW (ERP ≈ 27 MW) to 3.6 MW (ERP ≈1 GW) in 210 s and 35 steps and set at full power with 3.6 MW for 30 s. SIBS was observed by tuning the transmitter to 4.3 MHz (∼ $3f_{ce}$). The O-Mode HF beam was pointed to the azimuth angle of 202° and a zenith angle of larger than 21°. When the transmitter was turned on at 04:43 UT on 24 July 2011 with ERP ≈ 27 MW, the spectra do not show any emission lines. When the power exceeds 0.7 MW (ERP ≈ 190 MW) emissions are observed. The spectra then immediately showed downshifted and upshifted emissions at harmonics of f_{ci} as well as ion acoustic IA emission lines near 10 Hz. The discrete structures are attributed to SIBS instability and the IA emission lines are due to the Magnetized Stimulated Brillouin Scatter (MSBS) process [*Norin et al.*, 2009; *Bernhardt et al.*, 2009, 2010]. Figure 1 shows four snapshots of high resolution power spectrum for P_{heater} = 0.1 MW, P_{heater} = 0.7 MW, P_{heater} = 2 MW, and P_{heater} = 3.6 MW. This figure illustrates that increase of the pump power above 0.7 MW brings it above the threshold and turns on both the MSBS and SIBS process. As can be seen in Figure 1, when the power of the pump wave is near 0.7 MW (ERP ≈ 190 MW) the first few harmonics of the SIBS emission lines and much stronger IA emission line appear in the spectra. This shows that the IA emissions have lower threshold and larger growth rate in comparison with ion gyro-

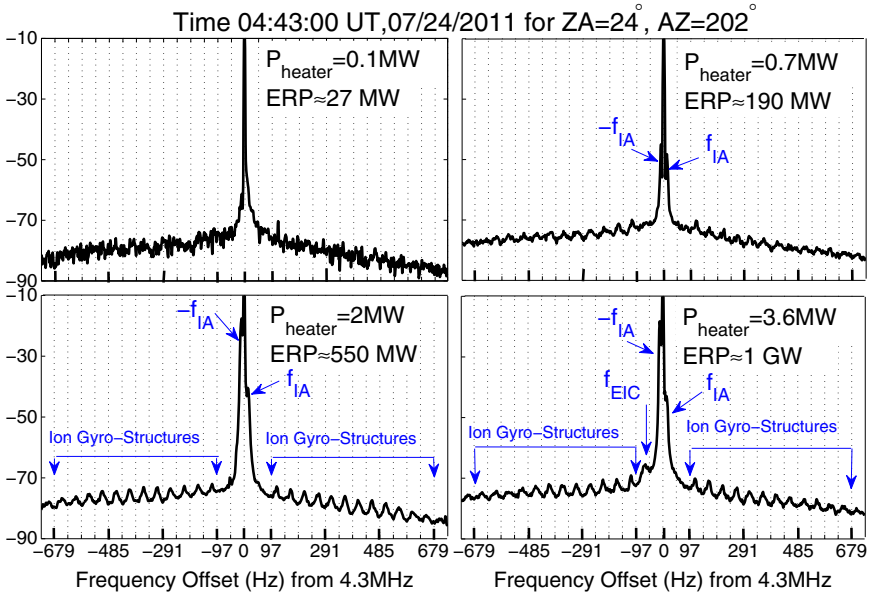

Figure 1. Stimulated Ion Bernstein Scatter (SIBS) with the transmitter tuned to $3f_{ce}$. Two other SEE emissions are observed within 10 Hz of the pump frequency as well as one emission line near 62 Hz generated by the MSBS process. Dotted lines at $f_{ci} \approx 48$ Hz. The threshold is near 0.7 MW for SIBS.

structures. Increasing power to 2 MW (ERP ≈ 550 MW) makes the IA lines much stronger and 10 harmonics of the SIBS appear clearly in upshifted and downshifted spectral emissions close to half multiples of the ion gyrofrequency near 48.5 Hz. The structures upshifted from the heater frequency correspond to the 2nd to 11th harmonics of the ion gyrofrequency, respectively. A distinct emission line appears in the spectra near 62 Hz for full power which is most likely the electrostatic ion cyclotron (EIC) mode generated through MSBS [*Bernhardt et al.*, 2009 and 2010]. Therefore, the IA line (MSBS process), ion gyro-harmonic lines (SIBS), and EIC line (MSBS process) have the thresholds of 0.4 MW (ERP ≈ 110 MW), 0.7 MW (ERP ≈ 190 MW) and 2.9 MW (ERP ≈ 800 MW), respectively. Therefore, IA line has the lowest threshold. It should be noted that in most of our observations, upshifted SIBS lines are stronger which is possibly because of weaker interaction of the upgoing pump wave than the down-going pump wave with the plasma, because of the raypaths. Detailed investigation is beyond the scope of this work and is the subject of future investigations. It should be noted that *D* region absorption of the HF wave is a nonlinear function of power. As a result, depending on ionospheric conditions (particularly the *D* region), different specific power thresholds may be observed.

[17] Figure 2 shows the spectrogram of SIBS for an experiment in which the pump power is varied during the heating cycle from 0.1 MW (ERP ≈ 27 MW) to 2 MW (ERP ≈ 550 MW). The first 40 s of the spectrogram corresponds to powers less than 0.7 MW (ERP ≈ 190 MW) and no emission lines exist. Almost all the SIBS emission lines appear above the noise level of the spectrum approximately 36 s after the heater was turned on. Thus, it could be inferred

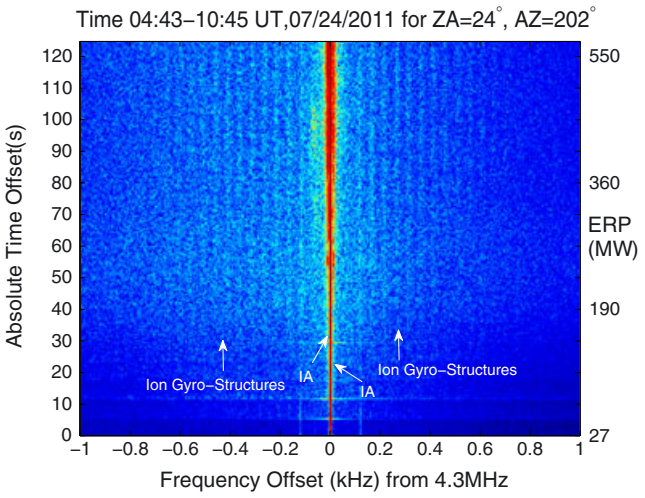

Figure 2. Time history of the SEE spectra of Stimulated Ion Bernstein Scatter (SIBS) associated with Figure 1. The pump power increased from 0.1 MW at t = 0 s in 0.1 MW steps every 6 s. The maximum value of power at end of cycle at 120 s is 2 MW.

that the pump field decays into different IB modes simultaneously rather than through a cascading process [e.g., *Zhou et al.*, 1994].

[18] A more extensive study of SIBS excited at $3f_{ce}$ was conducted during the 2012 campaign at HAARP. Figure 3 shows SEE spectra for the experiment carried out on 12 August 2012 from 4:30 UT to 5:30 UT. The transmitter was pointed at the magnetic zenith (ZA = 14°, AZ= 202°) and operated with O-mode polarization at full power alternating between 45 s at full power and 45 s off to allow recovery

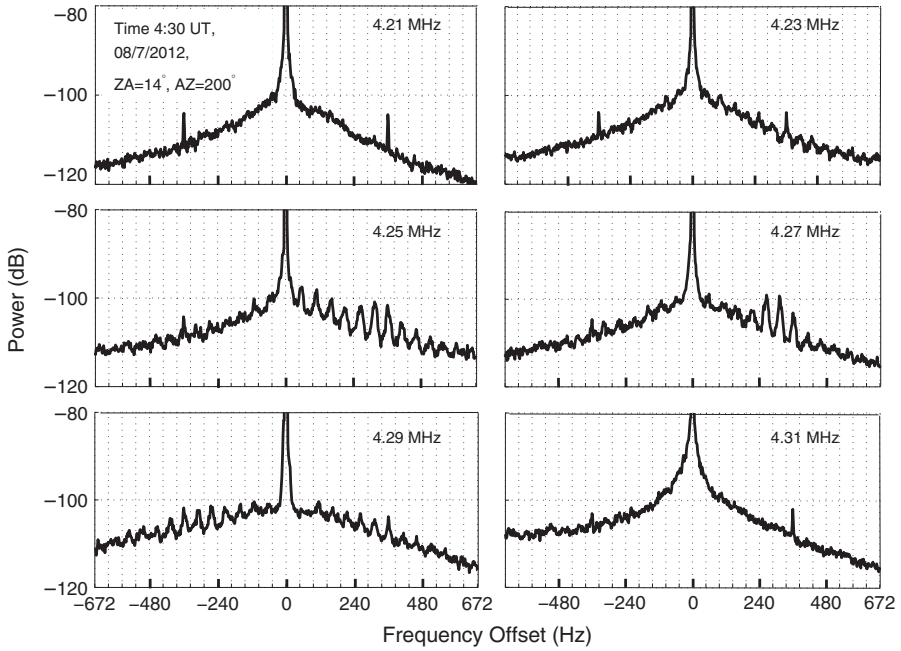

Figure 3. Stimulated Ion Bernstein Scatter (SIBS) with the transmitter tuned to $3f_{ce}$. Spectra showing SIBS for ZA = 14°, AZ = 202°, P_{heater} = 3.6 MW, and pump frequencies 4.21, 4.23, 4.25, 4.27, 4.29, and 4.31 MHz.

from artificially induced effects. The transmitter frequency stepped through $3f_{ce}$ from 4.21 to 4.31 MHz in 20 kHz steps every other "on" period to compare effects away and near $3f_{ce}$. According to the ionogram data, altitude of HF reflection was around 230 km during this experiment. The International Geomagnetic Reference Field (IGRF) model provided the magnetic field strength and direction in the upper atmosphere over HAARP. The magnetic field near the HF reflection altitude is estimated to be $|B| = 5.08210^{-5}$ T which results in $3f_{ce}$ approximately 4.26 MHz. No SIBS was observed for the pump frequency at 4.21 and 4.31 MHz which are far away from $3f_{ce}$. As the pump frequency gets closer to $3f_{ce}$, weak upshifted ion gyro-structures are observed at 4.23 MHz. SEE spectra show strong upshifted structures at 4.25 and 4.27 MHz which are shifted by approximately half harmonics of the ion gyrofrequency f_{ci}. The strongest lines are the seventh and fifth harmonics for 4.25 and 4.27 MHz, respectively. The structures extend up to 500 Hz above $3f_{ce}$. Symmetric upshifted and downshifted ion cyclotron harmonics appear in the spectra for the case of pump frequency tuned at 4.29 MHz. The behavior of SIBS with changing the pump frequency was investigated at larger angles relative to the MZ. A similar trend was observed at ZA = 18°, 24°, and 27°, except that IA and EIC emission lines also appear due to the excitation of the MSBS process. It should be noted that for the transmitter beam pointed at ZA = 21° only the MSBS process was excited.

[19] The effect of heater beam angle with respect to the magnetic zenith on the excited SIBS emission lines was examined during the campaign on 7 August 2012 from 4:30 UT to 5:30 UT and on 9 August 2012 from 4 UT to 5 UT. Figure 4 shows the SEE spectra for ZA = 14°, ZA = 18°, ZA = 24°, and ZA = 27°. The azimuth angle was fixed at 202° for all cases. The most clear excited SIBS was observed when the HF transmitter at HAARP was pointed at MZ. As can be seen, beam angle does not affect the most strongly excited SIBS emission line significantly since the most strongly excited line shifts only from fifth to seventh as the zenith angle changes from 14° to 18°. It turns out that for the zenith angles smaller than 18°, SIBS is the only parametric decay process. When the beam is tilted to an angle larger than 18°, the MSBS process occurs simultaneously producing intense IA emission lines.

[20] Considering the geometry of HAARP and location of the Kodiak SuperDARN radar, the signal transmitted by the Kodiak radar could be scattered only by electron density fluctuations in the direction normal to the magnetic field B. It has been shown that Langmuir waves propagate along B while UH waves propagate normal to B [*Hughes et al.*, 2003]. Therefore, the enhancement of the Kodiak SuperDARN radar signal is expected to be due to the interaction with UH waves. The first direct detection and observation of UH waves during O-mode heating of the ionosphere at HAARP was reported by *Hughes et al.* [2003]. The HF scattering mode detected by the Kodiak SuperDARN radar during the O-mode heating on 7 August 2012 from 4:30 UT to 5:25 UT is shown in Figure 5. The horizontal axis shows the time and vertical axis represents the slant range. This figure shows a strong correlation between the heating cycle of the HF transmitter and enhancement of the detected SuperDARN echoes. This figure corresponds to f_p variation from 4.17 to 4.33 MHz in 0.2 MHz steps during the heating cycle. The four beam angles shown correspond to those shown in Figure 4. Note the frequency 4.25 MHz denoted in each cycle in Figure 5 is the fixed frequency value used in the spectra of Figure 4. The strength of radar echoes increases significantly as the pump frequency increases from 4.27 MHz which is slightly larger than $3f_{ce}$. Simultaneous observations

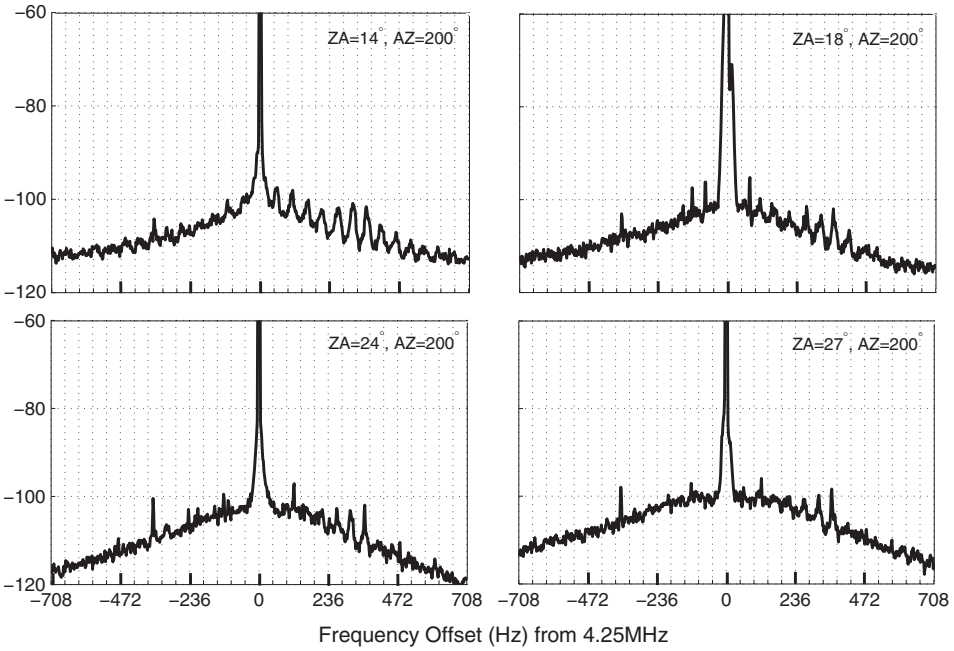

Figure 4. SIBS lines for ZA = 14°, ZA = 18°, ZA= 24°, and ZA = 27°. Heater beam pointed at MZ generates the strongest lines. The power spectrum corresponds to P_{heater} = 3.6 MW and pump frequency 4.25 MHz. IA emission lines at 10 Hz from the pump frequency appear for ZA = 18° generated through MSBS processes (off scale).

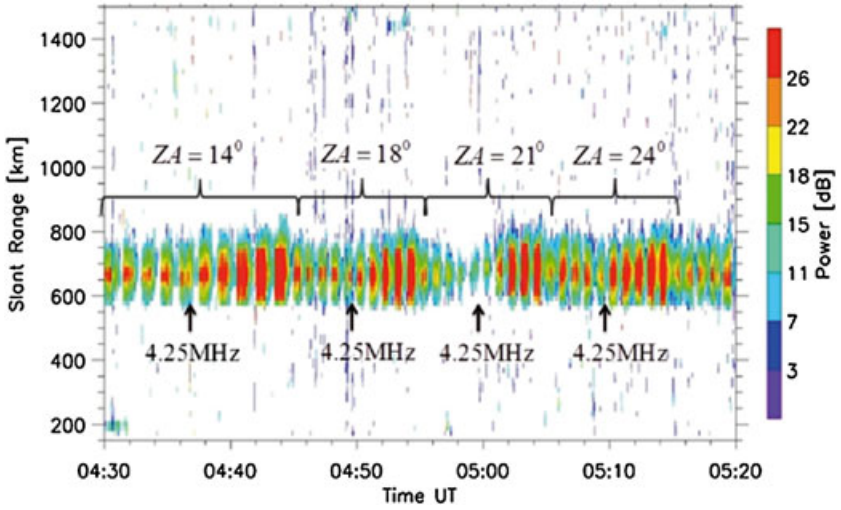

Figure 5. Artificial backscatter generated in the Kodiak SuperDARN radar during the ionospheric heating experiment on 7 August 2012. Beam angle was pointed at zenith angles 14°, 18°, 21°, and 24° and pump frequency was swept from 4.17 to 4.33 MHz. During the heating at MZ heater was on for 45 s and off for 45 s. During other experiments heater was on for 30 s.

of SuperDARN echoes and SIBS lines imply a theory of parametric decay instability which requires the decay of UH/EB waves to SIBS as described in section 4. It is important to note that previous observations indicate suppression of UH waves for f_p very near $3f_{ce}$ (within ≈30 kHz) during heating experiments [e.g., *Kosch et al.*, 2002 and references therein]. Unfortunately, frequency stepping used during the current experiments (0.2 MHz) did not have the resolution to investigate this suppression. This is planned for future experiments.

3.2. Associated Broadband SEE Features for $f_0 \approx 3f_{ce}$

[21] In this section, spectral features in a wider frequency band relative to the pump frequency are discussed and the relationship between these wideband features and the narrowband emission lines SIBS, IA and EIC (MSBS) is investigated. It is observed that the previously observed SEE downshifted peak (DP) feature [*Leyser*, 2001] and the newly discovered SIBS appear simultaneously in the SEE spectra which may show that these two features are produced by the same physical process but at different altitudes as a result of

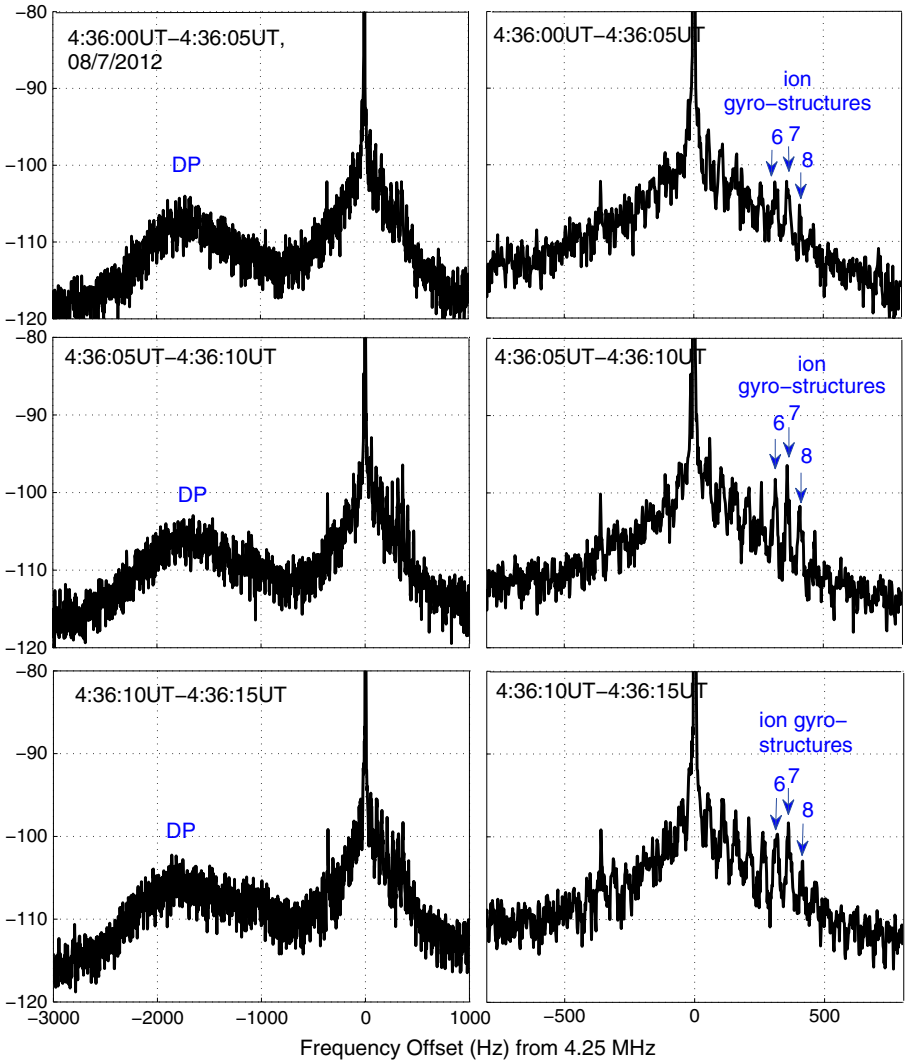

Figure 6. SEE spectra taken over 5 s intervals during 45 s heating demonstrate temporal evolution of DP (left panels) and SIBS emission lines (right panel). Note structures start to appear above the noise level approximately 6 s after the heater turn-on. Note that the sixth to eighth emissions lines have the fastest growth initially.

different propagation angle of the electrostatic waves relative to the magnetic field. The correlation of appearance of the so-called downshifted peak DP feature [*Leyser*, 2001] and SIBS has been observed for ZA = 14°, 18°, and 24°. The observed DP has frequency bandwidth between 700 Hz and 1.5 kHz. The temporal evolution of the spectrum for ZA = 14° is shown in Figure 6 and the power spectrum is taken over 5 s intervals during the heating process in which the heater power was 3.6 MW. The SEE spectra of emissions from 3kHz below the pump frequency to 1 kHz above are shown in the right panel in Figure 6, and the left panel shows the spectra in frequency range –600 to 600 Hz. According to this figure, DP appears in the spectra almost immediately after the heater turn-on while the spectra shows a slower growth for SIBS lines with time. Seventh to ninth lines appear above the noise level of the spectrum approximately 5 s after the heater was turned on. SIBS lines below the fifth harmonic appear in the spectra after 10 s. Further relationships between these features and the well known DP feature in SEE will be discussed in light of these recent observations. A power spectral maximum near 2kHz from the pump is observed.

[22] Since the SIBS and DP are correlated, DP, DM, and BUM can be used to estimate the proximity of the pump frequency to nf_{ce} just as the classical SEE features. Figure 7 shows variation of wideband spectral features with pump frequency. Considering that the DM vanishes as f_0 get closer to $3f_{ce}$, the DP can be used as an indicator of proximity of pump frequency to the gyro-frequency [*Tereshchenko et al.*, 2006]. During this experiment the average of the HF reflection altitude is about 210 km and $3f_{ce}$ is about 4.28 MHz. According to this figure, the DP gets very weak at 2.9 MHz. The UM and DM peaks become more pronounced for pump frequencies closer to $3f_{ce}$. Spectra shows the BUM peak as the pump frequency goes above 2.9 MHz which is expected from the theory that BUM should becomes stronger for

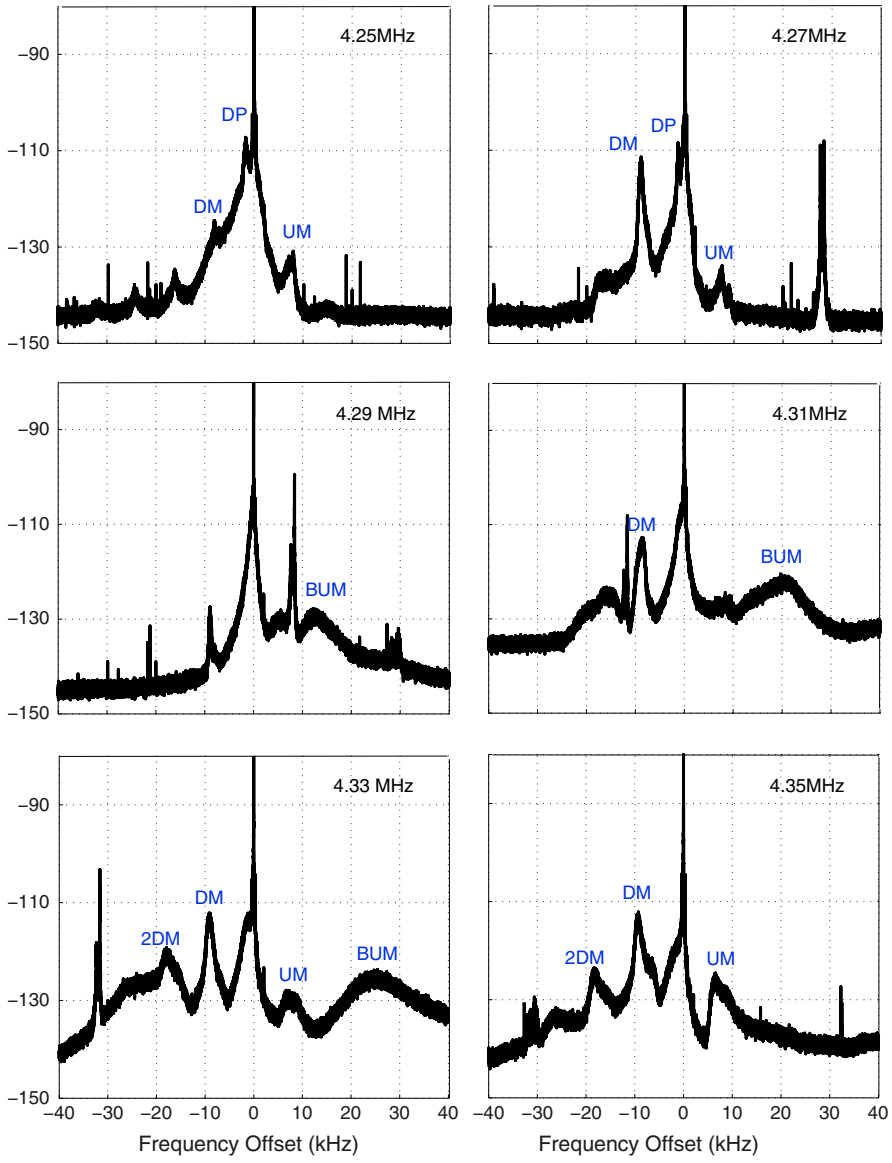

Figure 7. Variation of wideband SEE spectrum with the sweeping of the pump wave frequency near $3f_{ce}$. The spectra shows different classic SEE spectral features including the downshifted maximum DM (at –9 kHz), the upshifted maximum UM (at +9 kHz), and the broad upshifted maximum BUM (at +20 kHz). These are all observed simultaneously with the narrowband features of Figure 3.

$3f_{ce} \leq f_0 < 3f_{ce}$ + 100kHz [*Stubbe et al*., 1994; *Hussein et al*., 1998]. The offset frequency of the DP decreases from 1636 Hz to 1350 Hz as f_0 is increased from 4.25 MHz to 4.27 MHz which is consistent with the previous studies that f_{DP} decreases as pump frequency increases toward $3f_{ce}$ [*Huang and Kuo*, 1995].

3.3. Ion Gyro-Features and Pump-Induced Optical Emissions for $f_0 \approx 2f_{ce}$

[23] The SIBS for heating at $2f_{ce}$ was first investigated for a broad range of pump parameters by *Samimi et al.* [2012b]. During the 2012 campaign a set of experiments was dedicated to a more detailed study of SIBS with pump frequency sweeping through $2f_{ce}$ and $3f_{ce}$. This experiment aimed at considering the connection with pump-induced optical emissions and comparison of the cases with $f_0 = 2f_{ce}$ and $3f_{ce}$. Coordinated optical and SEE observations were carried out in order to provide a better understanding of electron acceleration and precipitation processes. Results for correlation between SEE SIBS emission lines and optical emissions is provided for pump heating near $2f_{ce}$ during the campaign. The observations affirm strong correlation between the SIBS and the pump-induced optical emissions.

[24] The transmitter frequency was tuned near the local $2f_{ce}$ at f_0 = 2.7 MHz for the first 60 s of the heating cycle and increased in 0.1 MHz every 30 s. According to the ionogram data, the reflection height for the transmitter frequency between 2.7 and 2.9 MHz is about 300 km which corresponds to $2f_{ce} \approx$ 2.76 MHz. The experiment was conducted

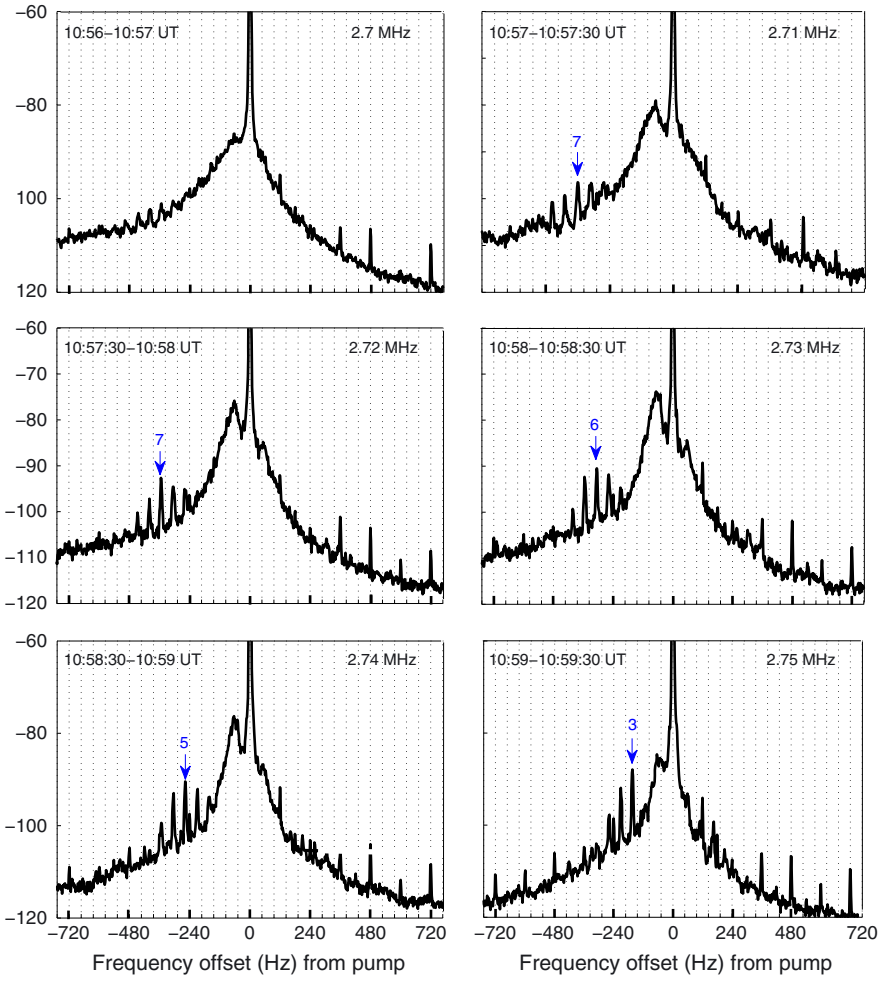

Figure 8. SEE Spectra showing SIBS for P_{heater} = 3.6 MW and f_0 being tuned near $2f_{ce} \approx 2.76$ MHz. Heater duty cycle is 30 s on, 30 s off and transmitter beam was pointed at MZ.

at night time on 9 August 2012 from 10:30 UT to 10:42 UT and 10:56 UT to 11:08 UT. The HF beam was pointed to the magnetic zenith with an azimuth of 202°and a zenith angle of 14°at full power (3.6 MW) during a 12 min heating cycle. The spectra shown in Figure 8 illustrate the variation of discrete SIBS lines with the pump frequencies 2.7, 2.71, 2.72, 2.73, 2.74, and 2.75 MHz. The spectra show weakly excited lines between the 7th and 10th harmonics for the pump frequency tuned at 2.7 MHz. Sixth to ninth lines appear in the spectra much stronger than the previous case at 2.71 and 2.72 MHz, and a strong emission line near 61 Hz also shows up in the spectra. This newly observed emission line could be related to observed optical emissions. Collision of accelerated electrons with neutral species may excite neutral particles and as a result produce pump-induced optical emissions. This is the subject of future investigation. It turns out that increasing the pump frequency toward $2f_{ce}$ moves the most strongly excited SIBS lines to lower harmonic numbers. The seventh, sixth, fifth, and third lines are the strongest for 2.72, 2.73, 2.74, and 2.75 MHz, respectively.

[25] First reports of pump-induced optical emissions came from Platteville [*Sipler and Biondi*, 1972; *Haslett and Megill*, 1974]. Artificially enhanced airglow due to excitation of oxygen atoms by accelerated electrons was also reported at Arecibo, Puerto Rico, by *Gordon and Carlson* [1974]. The electron acceleration is due to modified electron distributions by plasma waves such as Langmuir waves [*Weinstock*, 1975; *Isham et al.*, 1999a, 1999b] or UH resonance in the more recent study by *Kosch et al.* [2002]. Optical observations were carried out with multiple wide- and narrow-field systems at the HAARP site observing 557.7 and 630.0 nm emissions from atomic oxygen corresponding to >4.17 and >1.96 eV electron energy, respectively, and 427.8 nm N_2^+ emissions indicating ionization production at >18 eV. Figure 9a shows a series of optical images from looking up the magnetic field from HAARP (630.0 nm) during an artificial layer creation event and corresponding to Figure 8. The figure shows a clear correlation of airglow strength from 10:55 to 11:00 UT and SIBS lines (shown in Figure 8). As can be seen in Figure 9b, optical emissions are enhanced when strong SIBS lines begin to be observed in Figure 8 as the pump frequency is increased from 2.73 to 2.76 MHz. However, it should be noted that during another heating experiment near $2f_{ce}$ from 10:30 UT to 10:44 UT shown in Figure 9b, there were no SIBS lines associated with the optical emissions. These optical emissions are significantly stronger than during the subsequent experiment in which SIBS lines were observed. Therefore, the absence of SEE may possibly be explained by enhanced anomalous absorption associated with the enhanced electron

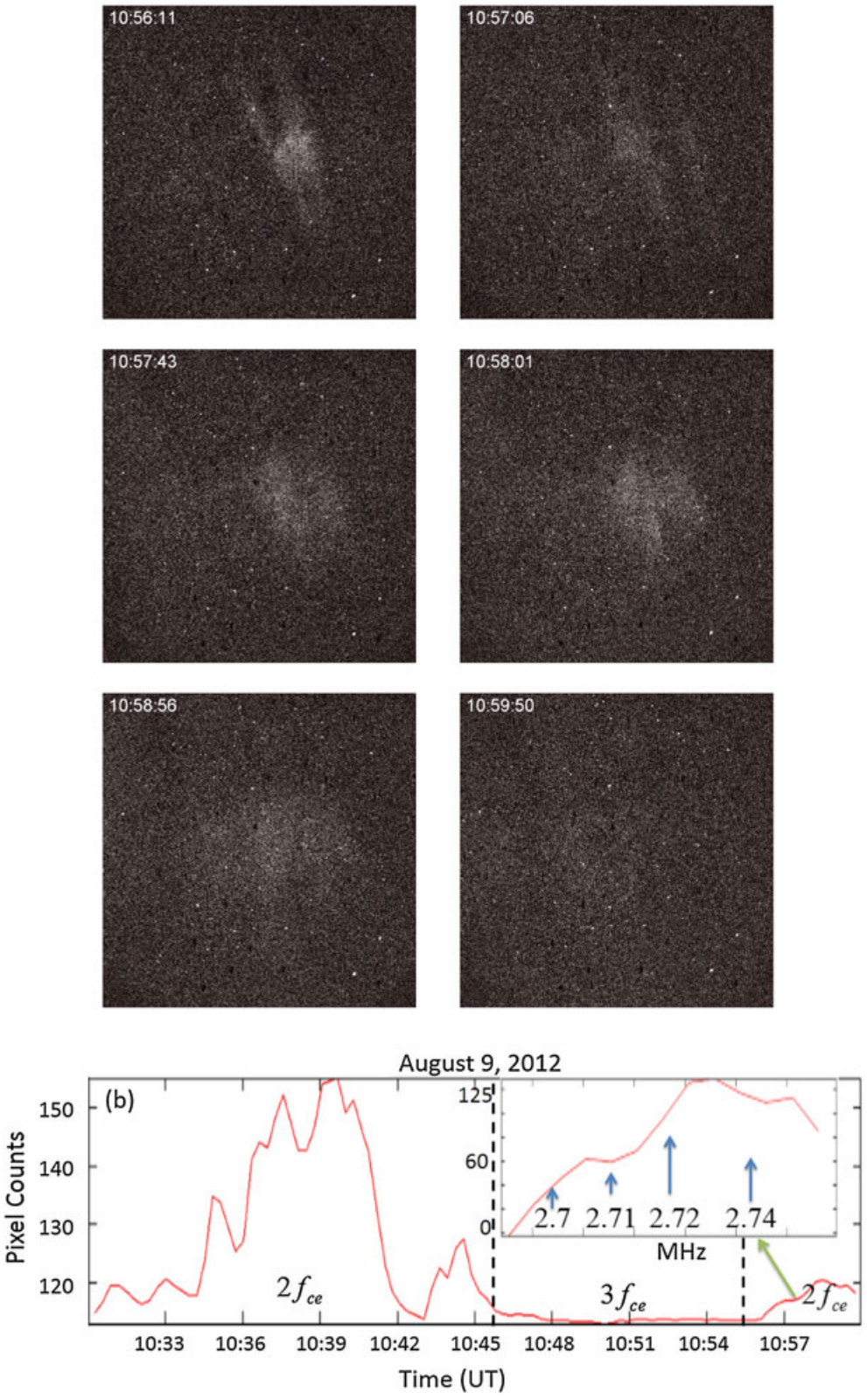

Figure 9. (a) Images of artificial optical emissions at 557.7 nm as viewed from the HAARP site looking up the magnetic field line with a 19° field of view (FOV) and (b) average 630.0 nm intensities for the central region of the 19° FOV images over time. The inserted figure corresponds to the observed SIBS lines shown in Figure 8. Vertical dashed lines show the time period of $3f_{ce}$ pump heating.

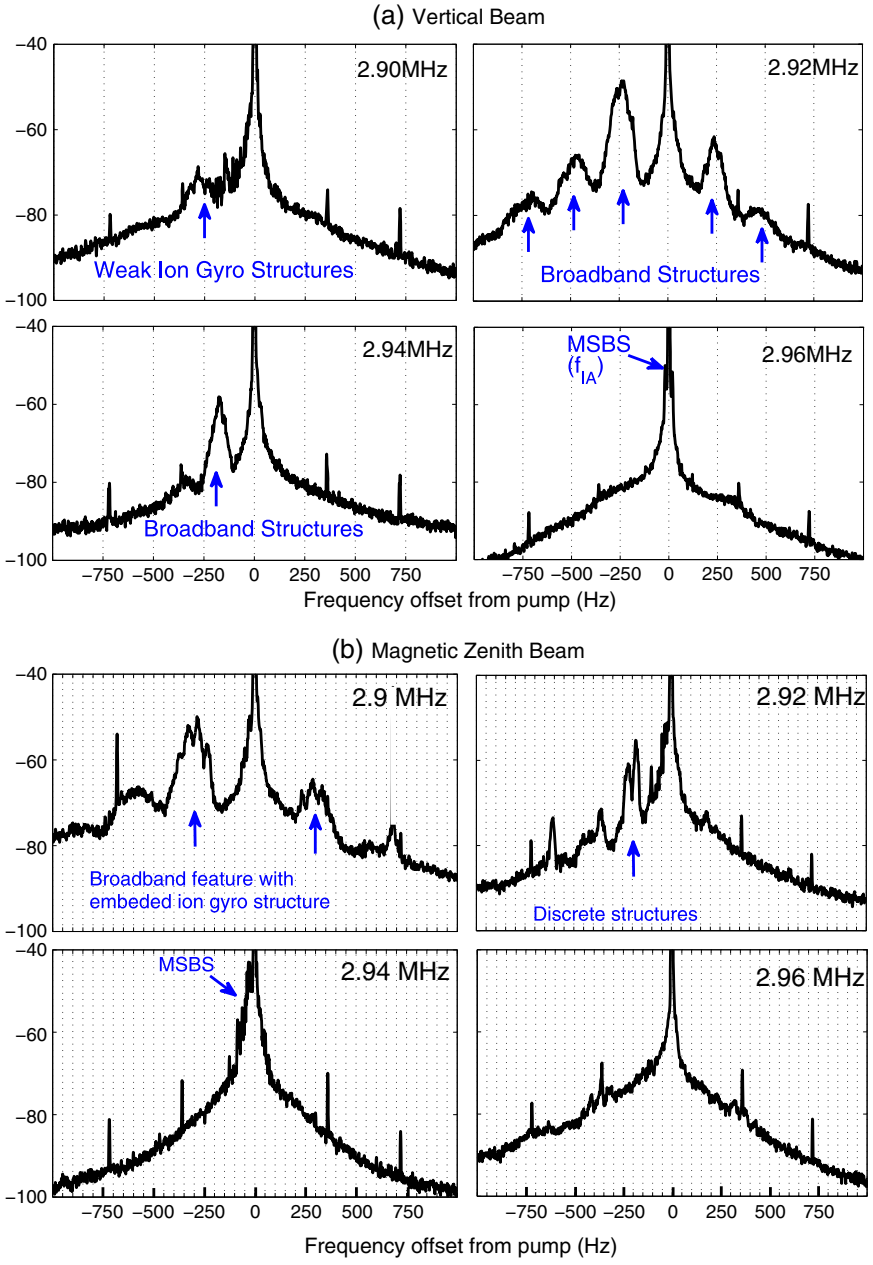

Figure 10. Experimental observations of broadband spectral features during which the heater frequency was tuned to 2.9, 2.92, 2.94, and 2.96 MHz and heating cycle was 30 s. Spectra also shows broadband spectral feature with embedded ion gyro harmonic structures at 2.9 MHz and for MZ beam. Dotted lines are at $f_{ci} \approx 50$ Hz and $2f_{ce} \approx 2.9$ MHz.

acceleration reducing the pump power delivered to the interaction region [*Weinstock*, 1975]. It is clear that further experiments are required to study the correlation between pump induced optical emissions and SIBS lines more carefully.

[26] In addition to the discrete SIBS emission lines, a possible variation of the previously observed broadband spectral feature was observed within 1 kHz of the pump frequency during the 2011 heating experiments near $2f_{ce}$. During this experiment the HF reflection height was 200 km and $2f_{ce} \approx 2.9$ MHz. This broadband spectral feature may be observed alone or with embedded discrete ion gyro-harmonic structures and due to parametric decay into oblique ion acoustic waves [*Samimi et al.*, 2012b]. Figure 10 demonstrates the broadband feature as well as discrete spectral feature for the experiment in which the heater was on for 60 s and off for 90 s at f_0 = 2.9, 2.92, 2.94, and 2.96 MHz. The transmitter beam was pointed at MZ and vertical. The data were obtained on 24 July 2011 when the HF wave was turned on at 11:48 UT. As can be seen in Figure 10a, the first broadband feature peaks at –235 Hz downshifted and +239 Hz upshifted from the pump frequency of 2.92 MHz for vertical beam. A second broadband spectral feature at –475 Hz and +460 Hz as well as a third broadband spectral feature at –760 Hz of the heater frequency were also observed. Increasing the pump frequency to 2.94 MHz suppresses the excited broadband spectral features such that

only a downshifted broadband feature is observed at -170 Hz. At frequencies far away from $2f_{ce}(\approx$ 2.9MHz), such as f_0 = 2.96 MHz spectra only shows emission lines at $\pm$19 Hz which is as a result of domination of the MSBS process. It has also been shown in the previous study by *Samimi et al.* [2012b] that the SIBS instability is stronger for the pump frequency near $2f_{ce}$.

[27] Figure 10b provides the spectra for a MZ beam that shows broadband spectral features at $\pm$270 Hz with embedded discrete ion gyro-structures for 2.9 MHz. As the pump frequency increases to 2.92 MHz only the third and fourth harmonics of discrete ion gyro-structures appear in the spectra and the broadband feature is suppressed. Similar to the previous case as the pump frequency gets further above $2f_{ce} \approx$ 2.9 MHz, the SIBS process vanishes and the MSBS process dominates at 2.94 MHz. No emission line associated with parametric decay instability is observed at 2.96 MHz.

4. Theory and Results

[28] In the SIBS process first the long wavelength electromagnetic (EM) wave is assumed to be converted to an electrostatic UH/EB pump wave and field aligned irregularities from the oscillating two stream instability (OTSI) [*Huang and Kuo*, 1995; *Dysthe et al.*, 1983]. The parametric decay instability then occurs which will be investigated here. The theory is based on the decay of the upper hybrid/electron Bernstein (UH/EB) pump wave into another UH/EB wave and neutralized/pure ion Bernstein (IB) waves. While the pure ion Bernstein wave propagates virtually perpendicular to the magnetic field, neutralized ion Bernstein waves propagate slightly off perpendicular ($k_\parallel/k_\perp > \sqrt{m_e/m_i}$) and have different dispersive characteristics due to Boltzmann electron behavior [*Chen*, 1984]. Here $k_\parallel$ and $k_\perp$ are the wave vector k parallel and perpendicular to the magnetic field and m_e and m_i are the electron and ion mass. The wave frequency and wave propagation direction are given by the energy and momentum conservation equations $\omega_0 = \omega_1 + \omega_S$, $k_0 = k_1 + k_S$ where (ω_0, k_0), (ω_1, k_1) and (ω_s, k_s) are the (radian) frequency and wave number for the pump, high frequency decay mode (UH/EB) and low frequency decay mode (IB/IA), respectively [*Kruer*, 1988; *Eliezer*, 2002] . The low frequency and high frequency waves are related with the following dispersion relation [*Porkolab*, 1974]:

$$\varepsilon(\omega_s) + \frac{\beta_e^2}{4}\chi_i(\omega_s)\left\{\frac{\varepsilon_e(\omega_s)}{\varepsilon_e(-\omega_L^*)} - 2\right\} = 0 \tag{1}$$

where β_e is the coupling coefficient, $\varepsilon(\omega) = 1 + \chi_e(\omega) + \chi_i(\omega)$, and $\varepsilon_e(\omega) = 1 + \chi_e(\omega)$. The susceptibility of the jth species is given by

$$\chi_j(\omega) = \frac{1}{k^2\lambda_{Dj}^2}\left\{\frac{1 + \zeta_{j0}\sum_{n=-\infty}^{+\infty}\Gamma_n(b_j)Z(\zeta_{jn})}{1 + \frac{i\nu_j}{k_\parallel v_{tj}}\sum_{n=-\infty}^{+\infty}\Gamma_n(b_j)Z(\zeta_{jn})}\right\} \tag{2}$$

where $b_j = k_\perp^2\rho_j^2$, k is the wave number, and ρ_j is the gyroradius. ζ_{jn} is given by

$$\zeta_{jn} = \frac{\omega + i\nu_j - n\Omega_n}{k_\parallel v_{tj}} \tag{3}$$

[29] v_{tj} is the thermal velocity, Ω_n is the gyrofrequency, ν_j is the collision frequency, $\Gamma_n(bj) = I_n(bj)\exp(-bj)$, Z is the Fried Conte function, and I_n is the first-order modified Bessel function. The coupling coefficient β_e is given by

$$\beta_e = \frac{e}{m_e}\left[\left(\frac{E_{0\parallel}k_\parallel}{\omega_0^2} + \frac{E_{0x}k_x + E_{0y}k_y}{\omega_0^2 - \Omega_{ce}^2}\right)^2 + \frac{(E_{0x}k_y + E_{0y}k_x)^2\Omega_{ce}^2}{\omega_0^2(\omega_0^2 - \Omega_{ce}^2)^2}\right]^{1/2} \tag{4}$$

[30] Considering the almost perpendicular propagation of Bernstein waves relative to the magnetic field, it is assumed that the interaction occurs at the upper hybrid resonance altitude. The dipole approximation ($k_0 \approx 0$) is used in this work where k_0 is the pump wave number. It should be noted that this is a simplified approach and the wave number of the pump field is more appropriately calculated by assuming a value determined from the scale size of irregularities generated from the oscillating two-stream instability [*Huang and Kuo*, 1995]. However, the simplified approach is adequate for initial characterization of the experimental data and more refined calculations will be pursued in future investigations. The pump field strength is described by the electron oscillating velocity $v_{osc} = eE_0/m_e\omega_0$ where e is the electron charge. The off-perpendicular angle between pump electric field and the background magnetic field is denoted by θ_E.

[31] Figure 11 demonstrates the influence of pump field strength (electron oscillating velocity) on the parametric decay instability for $\theta_E = 0.66°$ and $\omega_0 = 3\Omega_{ce} + 40\Omega_{ci}$. The left vertical axis is normalized frequency (blue lines); at the right is normalized growth rate (green lines) and the horizontal axis is the perpendicular normalized wave number. As can be seen, increasing the normalized oscillating velocity $\tilde{v}_{osc} = v_{osc}/v_{the}$ increases the number of destabilized modes from 5 up to 20 and changes the most excited modes from 4th to 15th. The fourth and fifth harmonics have the lowest threshold while according the previous study by *Samimi et al.* [2012b], and the second and third harmonics have the lowest threshold near the second electron gyroharmonic ($2\Omega_{ce}$). As in *Scales et al.* [2011] and *Samimi et al*. [2012a, 2012b], the wavelength is in the range $k_\perp\rho_{ci} \sim n$ where n is the harmonic number. The increase in $\tilde{v}_{osc}$ from 0.15 to 0.40 corresponds to electric field amplitude 3 V/m to $\sim$8 V/m. Such electric field amplitudes in the upper hybrid layer have been estimated to be in the range of 10 V/m by *Samimi et al.* [2012b] which is relevant to this investigation. They have also been estimated to be in the range of greater than 100 V/m by *Bernhardt et al.* [2009] at the reflection altitude.

[32] Variation of the parametric decay instability growth rate with pump frequency offset relative to $3\Omega_{ce}$ for $\theta_E = 0.66°$, $T_e/T_i = 4$, and $\tilde{v}_{osc} = 0.15$ is shown in Figure 12. The $\nu_{en} = 400$ Hz and $\nu_{in} = 1$ Hz are assumed. As the pump offset frequency increases further above and below the gyro-harmonic $3\Omega_{ce}$, the number of destabilized harmonics decreases. Increasing the offset frequency further

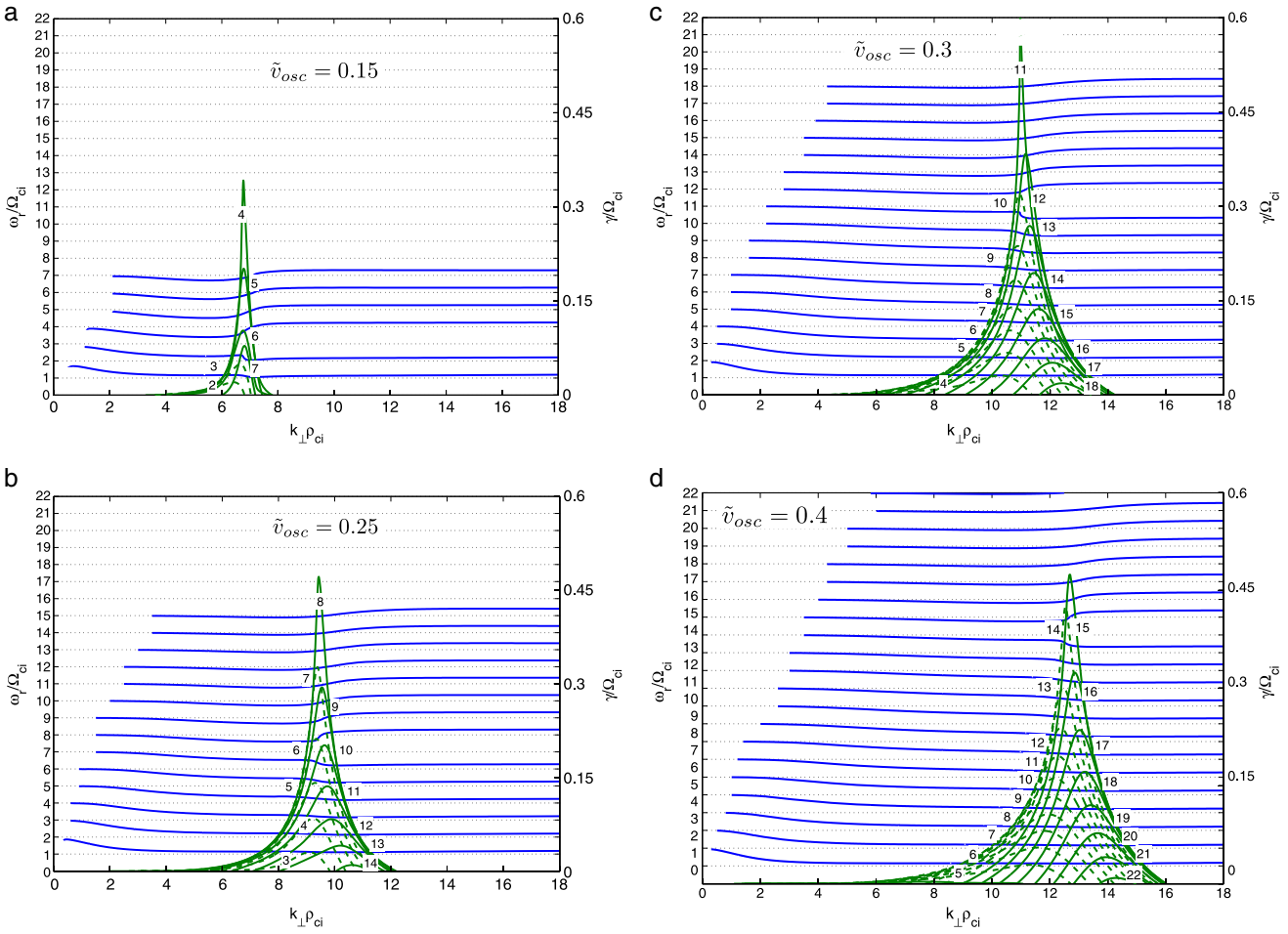

Figure 11. Dispersion relation of the low frequency decay mode (blue lines) and corresponding parametric decay instability growth rate (green lines) for $\theta_0 = 0.65$, $\omega_0 = 3\Omega_{ce}+5\Omega_{ci}$, $\nu_{in} = 3$ Hz, $\nu_{en} = 400$ Hz (a) $\tilde{v}_{osc} = 0.15$, (b) $\tilde{v}_{osc} = 0.25$, (c) $\tilde{v}_{osc} = 0.3$, and (d) $\tilde{v}_{osc} = 0.4$ obtained from equation (1). Note that as the pump strength increases more harmonics are destabilized.

above $3\Omega_{ce}$ also shifts the most excited mode toward the lower harmonics. The maximum growth rate of all destabilized harmonics from 1 to 19 is approximately the same for the pump frequency $\omega_0 = 3\Omega_{ce} - 30\Omega_{ci}$, and the maximum growth rate is obtained for offset frequency $20-30\Omega_{ci}$ above $3\Omega_{ce}$. Unstable harmonics excited by $\omega_0 < 3\Omega_{ce}$ are weaker. Therefore, whereas all harmonics are stable for frequency offset $50\Omega_{ci}$ below the gyro-harmonic, positive growth rate is obtained for lower harmonics with frequency offset up to $80\Omega_{ci}$ above $3\Omega_{ce}$. Therefore the theory is consistent with observations of enhancement of SIBS instability for the pump frequency being tuned to $2f_{ce}$ or $3f_{ce}$ from either below or above. Stepping the frequency through the gyro-harmonic from below to above shifts the most excited mode to the lower harmonics. This is also consistent with the observational data shown in Figure 3 that increasing f_0 from 4.25 to 4.27 MHz moves the strongest harmonic from seventh to fifth and no discrete emission lines were observed at 4.21 and 4.31 MHz since these frequencies are further away from $3f_{ce}$.

[33] Dispersive characteristics and growth rate as well as growth rate versus frequency of excited low frequency decay modes near $3\Omega_{ce}$ are shown in Figure 13 for three angles of pump field (a) $\theta_E = 0.5°$, (b) $\theta_E = 1°$, and (c) 2°. $\tilde{v}_{osc} = 0.13$, $T_e/T_i = 3$, and pump frequency is shifted by $5\Omega_{ci}$ above $3\Omega_{ce}$. The influence of θ_E on the most excited harmonic is negligible in comparison with offset of pump frequency relative to $3\Omega_{ce}$. It turns out that increasing the angle of pump field relative to the magnetic field reduces the growth rate significantly. This is also in agreement with experimental observations shown in Figure 4 that spectra show the strongest SIBS lines for magnetic zenith beam and variation of the most excited line with beam angle is negligible. It should be noted that angle of pump field in the ionosphere depends on the density of the ionosphere but it is expected to be roughly related to the transmitter beam angle.

[34] The correlation between the Downshifted peak DP and SIBS in Figure 6 suggests the DP is most likely due to parametric decay into an IA wave that is excited at larger θ_E [*Huang and Kuo*, 1995; *Samimi et al.*, 2012a, 2012b]. In fact, there is a possibility that the SIBS are produced at a different altitude than the DP as a result of smaller θ_E and parametric decay of UH/EB waves into low frequency pure/neutralized ion Bernstein modes. Figure 14 investigates the possibility of simultaneous parametric decay of the pump field into broadband oblique IA waves and discrete

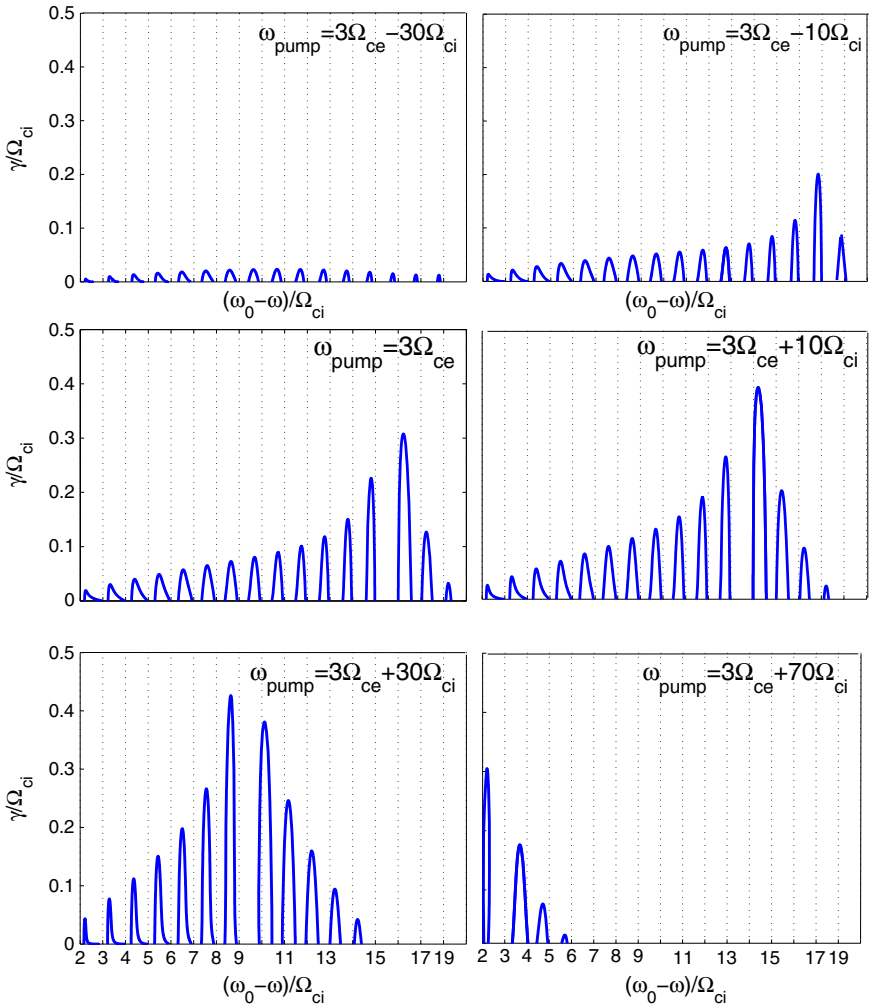

Figure 12. Growth rate versus frequency for θ_E = 0.66°, T_e/T_i = 4 and $\tilde{v}_{osc}$ = 0.15 obtained from equation (1). Pump frequency is varied near $3f_{ce}$ to show variation in growth rate of harmonics.

ion Bernstein waves at different altitudes which requires similar parameters except a different θ_E. Generation of an oblique IA mode in such plasma conditions was first proposed by [*Huang and Kuo*, 1995] and studied in particle-in-cell (PIC) simulations by *Hussein and Scales* [1997]. To reiterate, a similar process is proposed for $2f_{ce}$ heating [*Samimi et al.*, 2012a, 2012b] to explain the broadband spectral features as seen in Figure 10. Figure 14 shows the growth rate versus frequency for θ_E = 1.33° and 17.3° which correspond to the excited ion Bernstein modes and oblique IA mode, respectively. T_e/T_i = 7 and $\tilde{v}_{osc}$ = 0.1 are assumed in the calculations. At higher θ_E, highly oblique IA waves with dispersion relation $\omega \approx kc_s$ are destabilized instead of discrete neutralized IB modes. Comparison with experimental observations and results of the growth rate calculations suggests that the broadband spectral feature (DP) most likely involves this decay mode. The simultaneous occurrence of the broadband spectral feature (DP) and the discrete SIBS lines in Figure 6 most likely corresponds to the neutralized IB modes and oblique IA mode being generated at different altitudes.

[35] Discrete spectral lines are observed at smaller angle of electric field while there is no signature of the broadband mode. As can be seen, the first six harmonics correspond to SIBS lines and have frequency shift slightly below the harmonic of Ω_{ci} and involve the IB modes. The seventh harmonic has the highest growth rate. As shown in the right panel of Figure 14, the dispersion relation shows a broadband feature extending from $23\Omega_{ci}$ to $33\Omega_{ci}$ that corresponds to the frequency band 1.1–1.6 kHz as θ_E increases. This matches well with the experimental observations shown in Figure 6 that SIBS and DP (in frequency range 1.2–1.8 kHz) were observed at the same time. The predicted oblique IA wave from the theory appears in the frequency range 1.1–1.6 kHz. According to the Figure 6, the observed DP may have bandwidth up to 1 kHz in the frequency range 1–2 kHz. Some of this broadening may be due to higher order nonlinear processes that are not included in the theory presented in this work. It turns out that the ratio of electron temperature enhancement is the most effective parameter on the bandwidth of the excited oblique IA mode and increasing θ_E reduces the center frequency.

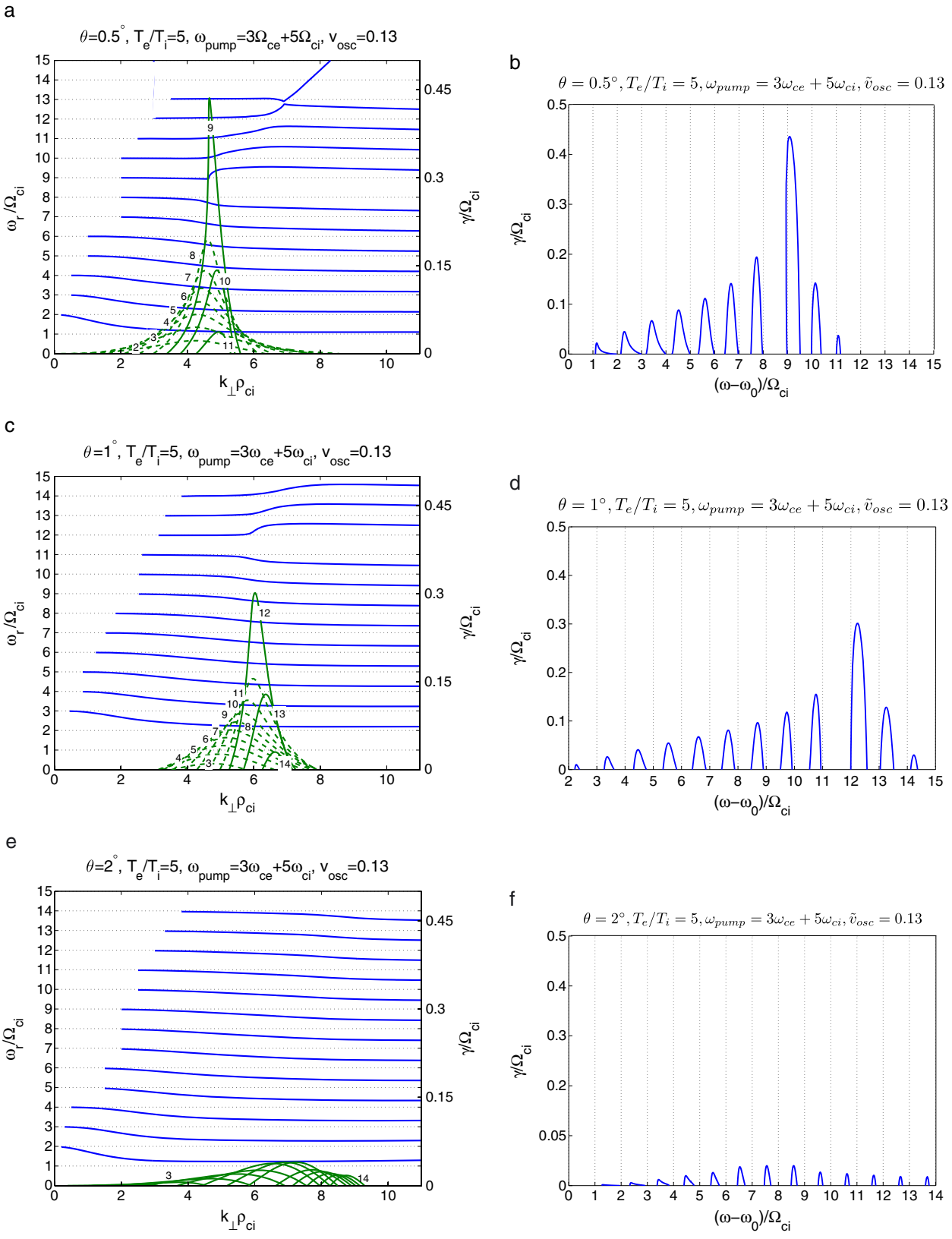

Figure 13. Dispersion relation for the low frequency decay mode (blue lines) and corresponding parametric decay instability growth rate (green lines) (left) and growth rate versus frequency for T_e/T_i = 5, $\omega_{\text{pump}} = 3\Omega_{ce} + 5\Omega_{ci}$, $\tilde{v}_{osc}$ = 0.13, ν_i = 3 Hz, and ν_e = 400 Hz, (a) θ_E = 0.5°, (b) θ_E = 1°, and (c)θ_E = 2°.

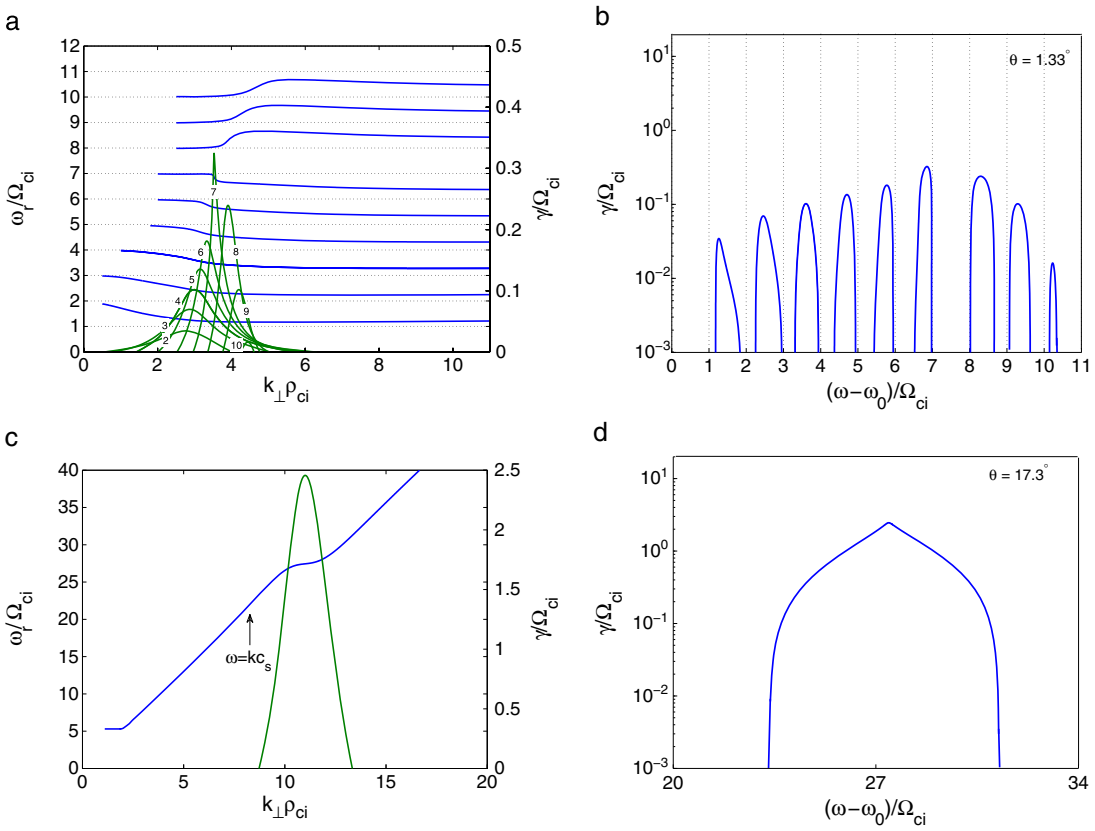

Figure 14. Growth rate versus frequency for θ_E = 1.33° and 17.3°. Top panel shows the dispersive characteristics and corresponding growth rate, and figures in the bottom represent the growth rate versus frequency. Note simultaneous parametric decay involving ion Bernstein and oblique ion acoustic modes at different angles of propagation to B that may allow both narrowband and wideband SEE as seen in Figure 6.

The previous work by *Samimi et al.* [2012b] also predicted oblique IA wave through parametric decay instability for $2f_{ce}$ heating and showed that IA waves can be excited at larger θ_E. However these broadband emission lines exist at a smaller frequency shift from the pump frequency as observed in Figure 10 and discussed in section 3.2. The IA growth rate is larger than the IB growth rate by a factor of 10 in Figure 14 which is consistent with the experimental observations shown in Figure 6 that DP appears in the spectra instantaneously after the pump turn-on while it takes about 10 s for SIBS lines to evolve and grow above the noise level.

5. Conclusions

[36] First observations of the discrete ion gyro-structures known as Stimulated Ion Bernstein Scatter (SIBS) in the SEE spectrum when the pump frequency is near $3f_{ce}$ have been presented. Coordinated observations of these SEE features and pump-induced optical emissions have also been presented. It is shown that increasing the heater power above 0.7 MW (ERP ≈ 190 MW) can excite SIBS at the HAARP facility at $3f_{ce}$. This threshold power is to be compared to an approximately 0.8 MW (ERP ≈ 66 MW) threshold power quoted for generation of SIBS for $2f_{ce}$ [*Samimi et al.*, 2012b]. Parametric decay of the UH/EB pump field into another UH/EB and IB waves in the upper hybrid altitude has been shown as a viable process for generation of these discrete ion gyro-harmonic structures in the SEE spectrum. Evidence of good correlation between SuperDARN backscatter and SIBS is observed when the pump frequency is in the vicinity of $3f_{ce}$ which implies UH waves as a driving source for SIBS. Variation of discrete spectral lines with the pump frequency stepping near the second and third gyro-harmonics and heater beam angle was studied during the experiment and observations show agreement with theoretical calculations. The excitation threshold of ion acoustic (IA) and electrostatic ion cyclotron (EIC) emission lines associated with magnetized stimulated Brillouin scatter (MSBS) also were measured. It turns out that SIBS lines have threshold of about 0.7 MW (ERP ≈ 190 MW), and IA and EIC lines appear in the spectra when pump power exceeds 0.4 MW (ERP ≈ 108 MW) and 3 MW (ERP ≈ 830 MW), respectively. A correlation of appearance and disappearance of the downshifted peak (DP) and SIBS lines for $3f_{ce}$ heating was observed. The theory suggests the decay of the UH/EB pump field into another UH/EB mode and a broadband oblique IA mode as a generation mechanism for the downshifted peak between 1.2 and 1.6 kHz that could occur at a different altitude relative to the SIBS generation region. It was shown that the IA mode (DP) grows faster than SIBS lines in both theory and experimental observations. Simul-

taneous observation of SIBS and airglow during heating near $2f_{ce}$ is presented which shows a correlation with the strength of optical emissions. This could shed light on the physical processes associated with artificial field alighted irregularities FAIs and electron precipitation.

[37] **Acknowledgments.** Some of this work was supported by the National Science Foundation. B.I. and O.V.-C. were supported by Army Research Office grants W911NF-11-0217 and W911NF-10-1-0002. The observations reported here were supported by the HAARP program through the Polar Aeronomy and Radio Science (PARS) Summer School. HAARP is a DoD program operated jointly by the U.S. Air Force and U.S. Navy. The authors wish to thank HAARP personnel for their assistance in designing this experiment and Bill Bristow for providing SuperDARN measurements.

References

Bernhardt, P. A., L. M. Duncan, and C. A. Tepley (1988), Artificial airglow excited by highpower HF waves, *Science*, *242*(4881), 1022.1027, doi: 10.1126/science.242.4881.1022.

Bernhardt, P. A., L. S. Wagner, J. A. Goldstein, V. Y. Trakhtengerts, E. N. Ermakova, V. O. Rapoport, G. P. Komrakov, and A. M. Babichenko (1994), Enhancement of stimulated electromagnetic emission during two frequency ionospheric heating, *Phys. Rev. Lett.*, *72*, 2879.

Bernhardt, P. A., C. Selcher, R. Lehmberg, S. Rodriguez, J. Thomason, M. McCarrick, and G. Frazer (2009), Determination of the electron temperature in the modified ionosphere over HAARP using the HF pumped Stimulated Brillouin scatter (SBS) emission lines, *Ann. Geophys.*, *27*, 4409–4427, doi:10.5194/angeo-27-4409-2009.

Bernhardt, P. A., C. Selcher, R. Lehmberg, S. Rodriguez, J. Thomason, M. McCarrick, and G. Frazer (2010), Stimulated Brillouin scatter in a magnetized ionospheric plasma, *Phy. Rev. Lett.*, *104*, doi: 10.1103/PhysRevLett.104.165004.

Bernhardt, P. A., C. A. Selcher, and S. Kowtha (2011), Electron and ion Bernstein waves excited in the ionosphere by high power EM waves at the second harmonic of the electron cyclotron frequency, *Geophys. Res. Lett.*, *38*, L19107, doi:10.1029/2011GL049390.

Bernhardt, P. A., L. M. Duncan, and C. A. Tepley (1988), Artificial airglow excited by high-power radio waves, *Science*, *242*, 1022–1027.

Chen, F. F. (1984), Introduction to plasma physics and controlled fusion, vol. 1, in *Plasma Physics*, 2nd ed., Springer.

Chilson, P. B., E. Belova, M. T. Rietveld, S. Kirkwood, and U. Hoppe (2000), First artificially induced modulation of PMSE using the EISCAT heating facility, *Geophys. Res. Lett.*, *27*, 3801–3804.

Dysthe, K. B., E. Mjolhus, H. L. Pecseli, and K. Rypdal (1983), A thermal oscillating two-stream instability, *Phys. Fluids*, *26*, 146, doi: http://dx.doi.org/10.1063/1.863993.

Eliezer, S. (2002), *The Interaction of High-Power Lasers With Plasmas*, Institute of Physics, Bristol, U. K.

Gordon, W. E., and Carlson Jr., H. C. (1974), Arecibo heating experiments, *Radio Sci.*, *9*(11), 1041–1047, doi:10.1029/RS009i011p01041.

Gustavsson, B., T. B. Leyser, M. Kosch, M. T. Rietveld, A. Steen, B. U. E. Brandstrom, and T. Aso (2006), Electron gyroharmonic effects in ionization and electron acceleration during high frequency pumping in the ionosphere, *Phys. Rev. Lett.*, *97*, 195002, doi: 10.1103/PhysRevLett.97.195002.

Haslett, J. C., and L. R. Megill (1974), A model of the enhanced airglow excited by RF radiation, *Radio Sci.*, *9* (11), 1005–1019, doi: 10.1029/RS009i011p01005.

Havnes, O., C. La Hoz, and L. L. Naesheim (2003), First observations of the PMSE overshoot effect and its use for investigating the conditions in the summer mesosphere, *Geophys. Res. Lett.*, *30*(23), 2229, doi: 10.1029/2003GL018429.

Hussein, A. A., and W. A. Scales (1997), Simulation studies of parametric decay processes associated with ionospheric stimulated radiation, *Radio Sci.*, *32*(5), 2099–2107, doi:10.1029/97RS01349.

Hussein, A. A., W. A. Scales, and J. Huang (1998), Theoretical and simulational studies of broad upshifted sidebands generation in the ionospheric stimulated radiation, *Geophys. Res. Lett.*, *25*, 955–958.

Huang, J., and S. P. Kuo (1995), A generation mechanism for the downshifted peak in stimulated electromagnetic emission spectrum, *J. Geophys. Res.*, *100*(A11), 21433–21438, doi:10.1029/95JA02302.

Hughes, J. M., W. A. Bristow, R. T. Parris, and E. Lundell (2003), SuperDARN observations of ionospheric heater-induced upper hybrid waves, *Geophys. Res. Lett.*, *30*(24), 2276, doi:10.1029/2003GL018772.

Hysell, D. L., and E. Nossa (2009), Artificial E-region field-aligned plasma irregularities generated at pump frequencies near the second electron gyroharmonic, *Ann. Geophys.*, *27*, 2711–2720, doi:10.5194/angeo-27-2711-2009.

Isham, B., M. T. Rietveld, T. Hagfors, C. La Hoz, E. Mishin, W. Kofman, T. B. Leyser, and A. P. van Eyken (1999a), Aspect angle dependence of HF enhanced incoherent backscatter, *Adv. Space Res.*, *24*, 1003–1006.

Isham, B., T. Hagfors, E. Mishin, M. Rietveld, C. LaHoz, W. Kofman, and T. Leyser (1999b), A search for the location of the HF excitation of enhanced ion acoustic and Langmuir waves with EISCAT and the Troms heater, *Radiophys. Quantum Electron.*, *42*, 607–618.

Kosch, M. J., M. T. Rietveld, A. J. Kavanagh, C. Davis, T. K. Yeoman, F. Honary, and T. Hagfors (2002), High-latitude pump-induced optical emissions for frequencies close to the third electron gyro-harmonic, *Geophys. Res. Lett.*, *29*(23), 2112–2115, doi:10.1029/2002GL015744.

Kosch, M. J., T. Pedersen, E. Mishin, S. Oyama, J. Hughes, A. Senior, B. Watkins, and B. Bristow (2007), Coordinated optical and radar observations of ionospheric pumping for a frequency pass through the second electron gyroharmonic at HAARP, *J. Geophys. Res.*, *112*, A06325, doi: 10.1029/2006JA012,146.

Kruer, W. L. (1988), *The Physics of Laser Plasma Interactions*, Addison-Wesley, New York.

Leyser, T. B., B. Thide, H. Derblom, A. Hedberg, and B. Lundborg (1989), Stimulated electromagnetic emission near electron cyclotron harmonics in the ionosphere, *Phys. Rev. Lett.*, *63*, 1145.

Leyser, T. B., B. Thide, H. Derblom, A. Hedberg, B. Lundborg, P. Stubbe, and H. Kopka (1990), Dependence of stimulated electromagnetic emission on the ionosphere and pump wave , *J. Geophys. Res.*, *95*(A10), 17233–17244, doi: 10.1029/JA095iA10p17233.

Leyser, T. B. (2001), Stimulated electromagnetic emissions by high-frequency electromagnetic pumping of the ionospheric plasma, *Space Sci. Rev.*, *98*, 223–328.

Mahmoudian, A., W. A. Scales, M. J. Kosch, A. Senior, and M. Rietveld (2011), Dusty space plasma diagnosis using temporal behavior of polar mesospheric summer echoes during active modification, *Ann. Geophys.*, *29*, 2169–2179, doi:10.5194/angeo-29-2169-2011.

Mahmoudian, A., and W. A. Scales (2012), Temporal evolution of radar echoes associated with mesospheric dust clouds after turn-on of radiowave heating , *J. Geophys. Res.*, doi:10.1029/2011JD017166.

Norin, L., S. M. Grach, T. B. Leyser, B. Thide, E. N. Sergeev, and M. Berlin (2008), Ionospheric plasma density irregularities measured by stimulated electromagnetic emission, *J. Geophys. Res.*, *113*, A09314, doi: 10.1029/2008JA013338.

Norin, L., T. B. Leyser, E. Nordblad, B. Thide, and M. McCarrick (2009), Unprecedentedly strong and narrow electromagnetic emissions stimulated by high-frequency radio waves in the ionosphere, *Phys. Rev. Lett.*, *102*(065003), doi:PhysRevLett 102.065003.

Pedersen, T. R., and E. A. Gerken (2005), Creation of visible artificial optical emissions in the aurora by highpower radio waves, *Nature*, *433*(7025), 498–500, doi:10.1038/nature03243.

Pedersen, T., B. Gustavsson, E. Mishin, E. Kendall, T. Mills, H. C. Carlson, and A. L. Snyder (2010), Creation of artificial ionospheric layers using high power HF waves, *Geophys. Res. Lett.*, *37*, L02106, doi: 10.1029/2009GL041895, 2010.

Pedersen, T., M. McCarrick, B. Reinisch, B. Watkins, R. Hamel, and V. Paznukhov (2011), Production of artificial ionospheric layers by frequency sweeping near the 2nd gyroharmonic, *Ann. Geophys.*, *29*, 47–51, doi: 10.5194/angeo-29-47-2011.

Porkolab, M. (1974), Theory of parametric instability near the lower-hybrid frequency, *Phys. Fluids*, *17*, 1432–1442, doi:10.1063/1.1694910.

Samimi, A., W. A. Scales, P. A. Bernhardt, S. J. Briczinski, C. A. Selcher, and M. J. McCarrick (2012a), On ion gyro-harmonic structuring in the stimulated electromagnetic emission spectrum during second electron gyro-harmonic heating, *Ann. Geophys.*, doi:10.5194/angeo-30-1587-2012.

Samimi, A., W. A. Scales, H. Fu, P. A. Bernhardt, S. J. Briczinski, and M. J. McCarrick (2012b), Ion gyro-harmonic structures in stimulated radiation during second electron gyro-harmonic heating: Part I theory, *J. Geophys. Res.*, doi:10.1029/2012JA018146.

Scales, W. A., M. R. Bordikar, A. Samimi, P. A. Bernhardt, S. Briczinski, C. A. Selcher, and M. McCarrick (2011), Observations and theory of ion gyro-harmonic structures in the stimulated radiation spectrum during second electron gyro-harmonic heating , *General Assembly and Scientific Symposium, URSI*, doi:10.1109/URSIGASS.2011.6051126.

Sipler, D. P., and M. A. Biondi (1972), Measurements of $O(^1D)$ quenching rates in the F region, *J. Geophys. Res.*, *77*, 6202–6212.

Stubbe, P., A. J. Stocker, F. Honary, T. R. Robinson, and T. B. Jones (1994), Stimulated electromagnetic emissions and anomalous HF wave

absorption near electron gyroharmonics, *J. Geophys. Res.*, *99* (A4), 6233–6246, doi:10.1029/94JA00023.

Tereshchenko, E. D., R. Yurik, Yu., B. Z. Khudukon, M. T. Rietveld, B. Isham, V. Belyey, A. Brekke, T. Hagfors, and M. Grill (2006), Directional features of the downshifted peak observed in HF-induced stimulated electromagnetic emission spectra obtained using an interferometer, *Ann. Geophys.*, *24*, 1819–1827, doi:10.5194/angeo-24-1819-2006.

Thide, B., H. Kopka, and P. Stubbe (1982), Observation of stimulated scattering of a strong high frequency radio wave in the ionosphere, *Phys. Rev. Lett.*, *49*, 1561–1564, doi:10.1103/PhysRevLett.49.1561.

Weinstock, J. (1975), Theory of enhanced airglow during ionospheric modifications, *J. Geophys. Res.*, *80* (31), 4331–4345, doi: 10.1029/JA080i031p04331.

Zhou, H. L., J. Huang, and S. P. Kuo (1994), Cascading of the upper hybrid/electron Bernstein wave in ionospheric heating experiments, *Phys. Plasmas*, *I*(9), 3044–3052, doi:http://dx.doi.org/10.1063/1.870929.